ADVANCES IN ATMOSPHERIC SCIENCES, VOL. 34, SEPTEMBER 2017, 1035–1046

• **Original Paper** •

Evaluating Common Land Model Energy Fluxes Using FLUXNET Data

Xiangxiang ZHANG[1], Yongjiu DAI[*2], Hongzhi CUI[1], Robert E. DICKINSON[3], Siguang ZHU[1], Nan WEI[1], Binyan YAN[3], Hua YUAN[2], Wei SHANGGUAN[2], Lili WANG[1], and Wenting FU[3]

[1]*College of Global Change and Earth System Science, Beijing Normal University, Beijing* 100875*, China*
[2]*School of Atmospheric Sciences, Sun Yat-sen University, Guangzhou* 510275*, China*
[3]*Department of Geological Sciences, the University of Texas at Austin, Austin, Texas* 78712*, USA*

(Received 13 October 2016; revised 2 May 2017; accepted 8 May 2017)

ABSTRACT

Given the crucial role of land surface processes in global and regional climates, there is a pressing need to test and verify the performance of land surface models via comparisons to observations. In this study, the eddy covariance measurements from 20 FLUXNET sites spanning more than 100 site-years were utilized to evaluate the performance of the Common Land Model (CoLM) over different vegetation types in various climate zones. A decomposition method was employed to separate both the observed and simulated energy fluxes, i.e., the sensible heat flux, latent heat flux, net radiation, and ground heat flux, at three timescales ranging from stepwise (30 min) to monthly. A comparison between the simulations and observations indicated that CoLM produced satisfactory simulations of all four energy fluxes, although the different indexes did not exhibit consistent results among the different fluxes. A strong agreement between the simulations and observations was found for the seasonal cycles at the 20 sites, whereas CoLM underestimated the latent heat flux at the sites with distinct dry and wet seasons, which might be associated with its weakness in simulating soil water during the dry season. CoLM cannot explicitly simulate the midday depression of leaf gas exchange, which may explain why CoLM also has a maximum diurnal bias at noon in the summer. Of the eight selected vegetation types analyzed, CoLM performs best for evergreen broadleaf forests and worst for croplands and wetlands.

Key words: model evaluation, Common Land Model, FLUXNET

Citation: Zhang, X. X., and Coauthors, 2017: Evaluating the Common Land Model energy fluxes using FLUXNET data. *Adv. Atmos. Sci.*, **34**(9), 1035–1046, doi: 10.1007/s00376-017-6251-y.

1. Introduction

Land surface processes, including the exchanges of energy, water vapor, momentum and carbon fluxes between the land surface and atmosphere, play important roles in determining changes in atmospheric circulations and the global climate. Surface energy fluxes, such as sensible heat flux (H_S), latent heat flux (H_L), net radiation (R_{net}), and ground heat flux (H_G), are fundamental components of the global energy equilibrium (Bonan, 2015); thus, their accurate estimation is critical for global climate change research. In recent years, much work has focused on the representation and evaluation of these energy fluxes (Roerink et al., 2000).

Land surface models (LSMs) are common tools to describe the aforementioned processes and provide lower boundary conditions for atmospheric general circulation models (Sellers et al., 1997). The first generation of LSMs consisted of only simple energy balance schemes. With increased physical knowledge, more sophisticated processes have been included in the current models, such as descriptions of land-based biogeochemical, biogeophysical and landscape processes (Oleson et al., 2013). The Common Land Model (CoLM) is a typical example. It contains improved treatments of soil moisture, soil temperature, turbulence fluxes, and other variables (Dai et al., 2003, 2004) and is based on a combination of an LSM (Bonan, 1996), the Biosphere–Atmosphere Transfer Scheme (Dickinson et al., 1986), and the Chinese Academy of Sciences Institute of Atmospheric Physics LSM (Dai and Zeng, 1997). Given the advantages of CoLM, it has been used as the land component in many fully coupled earth system models, such as the Community Climate Model from the National Center for Atmospheric Research (NCAR) (Zeng et al., 2002) and the Beijing Normal University-Earth System Model (BNU-ESM) (Ji et al., 2014). CoLM has also been used for some data assimilation schemes (Huang et al., 2008; Meng et al., 2009; Xu et al., 2011; Zhang et al., 2011).

Previous studies have demonstrated the excellent performance of CoLM. Xin et al. (2006) performed a validation experiment with CoLM at three arid stations with irrigated agriculture and demonstrated that the simulated results were

* Corresponding author: Yongjiu DAI
Email: daiyj6@mail.sysu.edu.cn

consistent with observations, especially in modeling the diurnal and annual changes of the vertical profiles of soil temperature. Ma et al. (2006) compared the regional evapotranspiration simulated by CoLM with remote sensing observations in China and concluded that CoLM can successfully simulate the magnitudes and spatial patterns of the monthly average evapotranspiration in China for certain months of 1991. In addition, Zheng et al. (2009) coupled CoLM with version 3 of the Regional Climate Model and found that the coupled model produced reasonable results for precipitation, near-surface air temperature, and general atmospheric circulation.

Given the critical role of LSMs in global climate research, an increasing number of researchers have evaluated these models (Stöckli et al., 2008; Blyth et al., 2010). From the early "Project for Inter-comparison of Land Surface Parameterization Schemes" (Henderson-Sellers et al., 1993) to the recent benchmark studies of LSMs (Luo et al., 2012; Best et al., 2015), the accuracy of LSMs has been greatly improved, especially after FLUXNET (Baldocchi et al., 2001) was established. For example, Stöckli et al. (2008) used FLUXNET to develop and validate the Community Land Model (CLM). Blyth et al. (2010) also evaluated Joint UK Land Environment Simulator energy fluxes using FLUXNET data.

A good model should depict physical processes on different spatial and temporal scales based on different climate backgrounds. Despite the above studies, CoLM has not yet been sufficiently studied to verify its performance for different vegetation types in various climate zones. FLUXNET provides a useful dataset for the development of LSMs (Baldocchi et al., 2001), and this product can be used to evaluate the performance of CoLM for different biomes.

In this study, we focused on the evaluation of land surface energy fluxes, such as H_S, H_L, R_{net} and H_G, as simulated by CoLM. This is the initial phase of a broader research effort by our group, as the accurate simulation of energy fluxes is a central premise of a good LSM. This work was conducted for ten different climate zones and eight different land-cover types. Simulations with different timescales were analyzed first, and then the results for several specific land-cover types from different climate zones were examined.

2. Methods

2.1. *Model description*

The initial version of CoLM was developed as a state-of-the-art LSM for climate studies. Two versions of this model have been developed based on the first version. One is CLM, developed by NCAR, which was first coupled with version 3 of the Community Climate Model, then with version 2 of the Community Atmosphere Model, and is currently coupled with the Community Earth System Model (Bonan et al., 2002; Zeng et al., 2002; Oleson et al., 2008). The other is the current version of CoLM, developed at BNU (Dai et al., 2003, 2004), which has been coupled with BNU-ESM (Ji et al., 2014). The two coupled models participated in phase 5 of the Coupled Model Intercomparison Project and provided projections of future climate for the IPCC's Fifth Assessment Report.

CoLM utilizes an improved two-stream approximation model for calculating canopy radiation and a two-big-leaf (Dai et al., 2004) model, which considers shaded leaves and sunlit leaves separately. Its performance in simulating stomatal conductance, photosynthesis, and leaf temperature has been improved relative to the earlier version of CoLM. In CoLM, energy fluxes are computed by solving the energy balance equation at the land–atmosphere interface (Dai et al., 2003), which is expressed by Eq. (1), given the following three assumptions:

(1) Convective heat transfer is assumed to be negligible within the canopy, soil and snow layers;

(2) Vaporization and sensible heat transfer are assumed to be negligible within the snow and soil layers;

(3) Heat conductance is assumed to be negligible within the canopy.

$$c\Delta z\frac{\mathrm{d}T}{\mathrm{d}t} = R_{net} - H_S - H_L \tag{1}$$

In Eq. (1), c is volumetric heat capacity, Δz is the depth of the soil layer, T is the soil temperature, and the net radiation R_{net} is the sum of the net shortwave radiation ($R_{net,s}$) and net longwave radiation ($R_{net,l}$):

$$R_{net} = R_{net,s} + R_{net,l}\,, \tag{2}$$

$$R_{net,s} = S\downarrow(1-\alpha)\,, \tag{3}$$

$$R_{net,l} = aL\downarrow + b\sigma T_c^4 + d\sigma T_g^4\,. \tag{4}$$

In Eqs. (3) and (4), $S\downarrow$ denotes downward solar radiation; α is albedo; $L\downarrow$ denotes downward longwave radiation; T_c denotes canopy temperature; T_g denotes ground temperature; and a, b and d are parameters related to the fraction of the vegetated area and emissivity of the ground.

The turbulent heat fluxes H_S and H_L are calculated as the heat resistance multiplied by the temperature/water gradient, and are described by Eqs. (5) and (6), respectively:

$$H_S = r(T_c - \theta_a)\,, \tag{5}$$

$$H_L = r(q_c - q_a) + E_w + E_{tr}. \tag{6}$$

In Eqs. (5) and (6), r denotes heat resistance; E_w denotes evaporation from the ground; E_{tr} denotes transpiration; θ_a stands for air temperature; and q_c and q_a are the specific humidity of the canopy and atmosphere, respectively.

2.2. *FLUXNET*

FLUXNET is a network of globally distributed flux towers that measure the energy, water vapor, and carbon dioxide exchanges between the land surface and atmosphere, using eddy covariance methods. Currently, FLUXNET consists of more than 800 sites, covering a variety of biome types and climate zones (Baldocchi et al., 2001, 2016). FLUXNET provides the most comprehensive dataset of the terrestrial ecosystem, and its measurement uncertainties can be accurately quantified at different levels. The released datasets cover eleven land cover types, based on information from

the International Geosphere–Biosphere Programme, and seventeen subclasses of the five main classes of climate zones (Kottek et al., 2006).

To evaluate the performance of CoLM for different vegetation types in different climate zones, we selected sites that represented different vegetation types, allowing cases of as many climate zones as possible to be considered. For example, the grassland (GRA) sites cover three of the main climate zones [B (arid), C (warm-temperate), and D (snow)] and five subclasses [warm temperate climate with hot summer (Cfa), temperate climate with warm summer (Cfb), snow climate with warm summer (Dfa), steppe climate (BSk), and warm temperate climate with dry summer (Csa)]. In this study, eight vegetation types were included: cropland (CRO), deciduous broadleaf forest (DBF), evergreen broadleaf forest (EBF), evergreen needleleaf forest (ENF), wetland (WET), GRA, mixed forest (MF) and savanna (SAV).

The selected sites also meet the requirements of having data that cover at least two continuous years, and containing few gaps. Ultimately, twenty FLUXNET sites covering eight plant function types and ten climate zone subclasses were chosen, and their locations, data coverage, and climate information are listed in Table 1.

2.3. *Atmospheric forcing and parameters*

CoLM requires eight atmospheric forcing variables for offline simulations: downward solar radiation at the surface (W m^{-2}); downward longwave radiation (W m^{-2}); precipitation (mm s^{-1}); temperature at the reference height (K); wind speed in both the eastward and northward directions (m s^{-1}); atmospheric pressure at the surface (Pa); and specific humidity at the reference height (kg kg^{-1}). Five times the length of the observational record was used for model spin-up to provide stable initial conditions. All forcing data used in this research were in-situ measurements from FLUXNET.

We utilized the improved MODIS Leaf Area Index (LAI) products (Yuan et al., 2011) for each site with consistent land-cover type settings in the model. The other land surface characteristic datasets and soil and vegetation properties were set to their default values; the parameters for the different sites were not optimized. All analyses are based on the original output.

Table 1. FLUXNET site descriptions and climatology (Climate class and climate group are defined according to Koppen climate classification, *P* for precipitation, *T* for mean temperature, Lat and Lon for latitude and longitude, Years for the period with observations, Land cover types are defined by USGS classification.).

ID	Site	Climate class	Climate group	LAI	*P* (mm yr^{-1})	*T* (°C)	Lat	Lon	Years	Land-cover category (USGS)
1	US-Bo1	Dfa	Temperate-continental with hot summers	5–5.5	991	11.0	40.0°N	88.3°W	1997–2006	Cropland
2	FR-Hes	Cfb	Temperate	–	793	9.2	48.7°N	7.1°E	2001–06	Deciduous broadleaf forest
3	IT-Ro1	Csa	Subtropical-Mediterranean	3.03	764	15.4	42.4°N	11.9°E	2002–06	Deciduous broadleaf forest
4	US-Ha1	Dfb	Temperate-continental with warm summers	3.53	1071	6.6	42.5°N	72.2°W	1994–2001	Deciduous broadleaf forest
5	AU-Tum	Cfb	Temperate	2.4	1159	10.7	35.7°S	148.2°E	2002–05	Evergreen broadleaf forest
6	DE-Tha	Cfb	Temperate	8	643	8.1	51.0°N	13.6°E	1998–2005	Evergreen needleleaf forest
7	FI-Hyy	Dfc	Boreal	6.7	620	2.2	61.8°N	24.3°E	2001–04	Evergreen needleleaf forest
8	US-Blo	Csa	Subtropical-Mediterranean	4.63	1380	11.2	38.9°N	120.6°W	2000–06	Evergreen needleleaf forest
9	CA-Mer	Dfb	Temperate-continental with warm summers	1.3	891	6.1	45.4°N	75.5°W	1999–2005	Wetland
10	FI-Kaa	Dfc	Boreal	–	454	−1.4	69.1°N	27.3°E	2004–05	Wetland
11	IT-Amp	Cfa	Subtropical-Mediterranean	2.13	945	10.6	41.9°N	13.6°E	2003–06	Grassland
12	NL-Ca1	Cfb	Temperate	11.3	777	9.6	52.0°N	4.9°E	2003–06	Grassland
13	US-Bkg	Dfa	Temperate-continental with hot summers	0.2–3	586	6.0	44.3°N	96.8°W	2005–06	Grassland
14	US-FPe	BSk	Dry (arid and semi-arid)	2.5	335	5.5	48.3°N	105.1°W	2000–06	Grassland
15	US-Var	Csa	Subtropical-Mediterranean	1.2	544	15.9	38.4°N	121.0°W	2001–06	Grassland
16	US-Syv	Dfb	Temperate-continental with warm summers	4	826	3.8	46.2°N	89.3°W	2002–05	Mixed forest
17	AU-How	Aw	Tropical	2.4	1449	27.0	12.5°S	131.2°E	2002–05	Savanna
18	BW-Ma1	BSh	Dry (arid and semi-arid)	0.9–1.3	493	22.4	19.9°S	23.6°E	1999–2001	Savanna
19	ES-LMa	Csa	Subtropical-Mediterranean	–	370	16.5	39.9°N	5.8°W	2004–06	Savanna
20	ZA-Kru	Cwa	Subtropical-Mediterranean	1.7	525	22.2	25.0°S	31.5°E	2002–03	Savanna

2.4. *Correction of measurements*

To resolve the imbalance issue of the surface energy budgets (Wilson et al., 2002), which refers to the inconsistencies of the independent measurements of the major energy balance flux components, we adjusted H_S and H_L and assumed that the measured Bowen ratio was correct. The tuning equations are as follows:

$$H_{S,cor} = AH_{S,u} = \frac{R_{net} - H_G}{H_{S,u} + H_{L,u}} H_{S,u} \quad (7)$$

$$H_{L,cor} = AH_{L,u} = \frac{R_{net} - H_G}{H_{S,u} + H_{L,u}} H_{L,u} \ . \quad (8)$$

In Eqs. (7) and (8), the variables with the subscript cor denote the corrected variables, and those with u indicate the uncorrected variables. The tuning factor A will make up the under-measurement of H_S and H_L. When H_G is missing, the alternative factor A^* is used and is expressed as $A^* = R_{net}/(H_{S,u} + H_{L,u})$ (Twine et al., 2000). The corrected surface energy fluxes for the FLUXNET observations were used to validate the model in this study.

In this research, the alternative factor A^* was applied only to sites US-Ha1 and FI-Hyy of the 20 selected sites. The vegetation type of US-Ha1 is deciduous broadleaf forest and that of FI-Hyy is evergreen needleleaf forest, both of which are prone to small H_G because of dense vegetation. In general, the method may have its limitations, but the lack of a surface energy balance has troubled the research community for a long time. Twine et al. (2000) reviewed the surface fluxes and energy-balance closure, discussed improved energy-balance methods, and then suggested that the Bowen-ratio closure method may be the most appropriate. This Bowen-ratio closure method has been widely used; Jung et al. (2010) even used it to process 253 globally distributed flux towers when producing a global evapotranspiration dataset. As the Bowen-ratio method may not always be ideal at a specific site, its rationale should be re-evaluated when further validation at specific sites is performed.

2.5. *Decomposition method*

In this study, both the simulated and observed results were decomposed into three parts: annual cycle, daily residuals, and diurnal bias (stepwise perturbation), as described by Eq. (9):

$$X_i = X_m + X_d + X_s \ . \quad (9)$$

In Eq. (9), X_i stands for the simulation or observation at each time step, X_m stands for the monthly average of the month in which X_i is observed, X_d is calculated as the average over the entire corresponding day, and X_s is the residual when the monthly mean and daily mean are removed from X_i. The data used for the calculation of X_d are equal to the averages of the original values minus their corresponding monthly means. Taking one day in May as an example, there were 48 values within this single day, i.e., $X_i = X_1, X_2, X_3, \ldots, X_{48}$. X_m is the monthly average for May, such that $X_d = 1/48 \sum_1^{48}(X_i - X_m)$. The annual cycle, which is composed of the monthly averages, can capture seasonal issues, such as the deficiencies in modeled vegetation phenology or soil drying after wet seasons, by identifying the times that the model may produce biases. Similarly, the diurnal cycle, which consists of hourly averages, enables the identification of the particular time in a given day that a model underperforms. The diurnal cycles for different seasons were analyzed in this research to evaluate the performance of CoLM under different vegetation types during different stages of vegetation growth and water availability.

2.6. *Data analysis*

Three statistical indexes—the correlation coefficient (R), the variance ratio, and the root-mean-square error (RMSE)—were summarized within a Taylor diagram (Taylor, 2001) to evaluate the model performance. The Taylor diagram was used to check the performance of CoLM in simulating the surface energy fluxes from stepwise, to daily, to monthly averages, and thus indicated how the model performance differed at different timescales.

Quantitative measurements of the differences between the simulations and observations are recommended to evaluate the performance of hydrological models (Aitken, 1973; James and Burges, 1982). RMSE, R, and the normalized bias (N_{bias}) were used as the statistical performance criteria in the evaluation of this work. N_{bias} is the bias between the model simulation and observational data normalized by the downward solar radiation at the same time step, as shown in Eq. (10).

$$N_{bias} = \frac{X_{model} - X_{obs}}{R_{solar}} \ . \quad (10)$$

Because the solar radiation should not be zero (since it is in the denominator), all N_{bias}-based analyses are restricted to the daytime.

3. Results

As mentioned earlier, this study seeks to evaluate the performance of CoLM in simulating the surface energy fluxes for various vegetation types in multiple climate zones. In this section, the general model performance for simulating H_S, H_L, and R_{net} on different timescales is assessed using all three indexes (R, RMSE, and N_{bias}). The performance of CoLM for four specific land-cover types is then discussed separately to observe how the model performs for different climate zones and a given vegetation type.

3.1. *Different timescales*

The comparisons between the observed and simulated H_S, H_L, and R_{net} values shown in Fig. 1 and Table 2 reflect the performance of the model across different timescales—namely, stepwise, daily, and monthly. The Taylor diagrams show that the R values of H_S, H_L, and R_{net} mostly vary from 0.6 to 0.95, 0.7 to 0.95, and 0.95 to 1.0, respectively, and the normalized standard deviations of the three fluxes mostly vary from 0.9 to 1.5, 0.7 to 1.2, and 0.9 to 1.2, respectively. Obviously, the overall variability (normalized standard

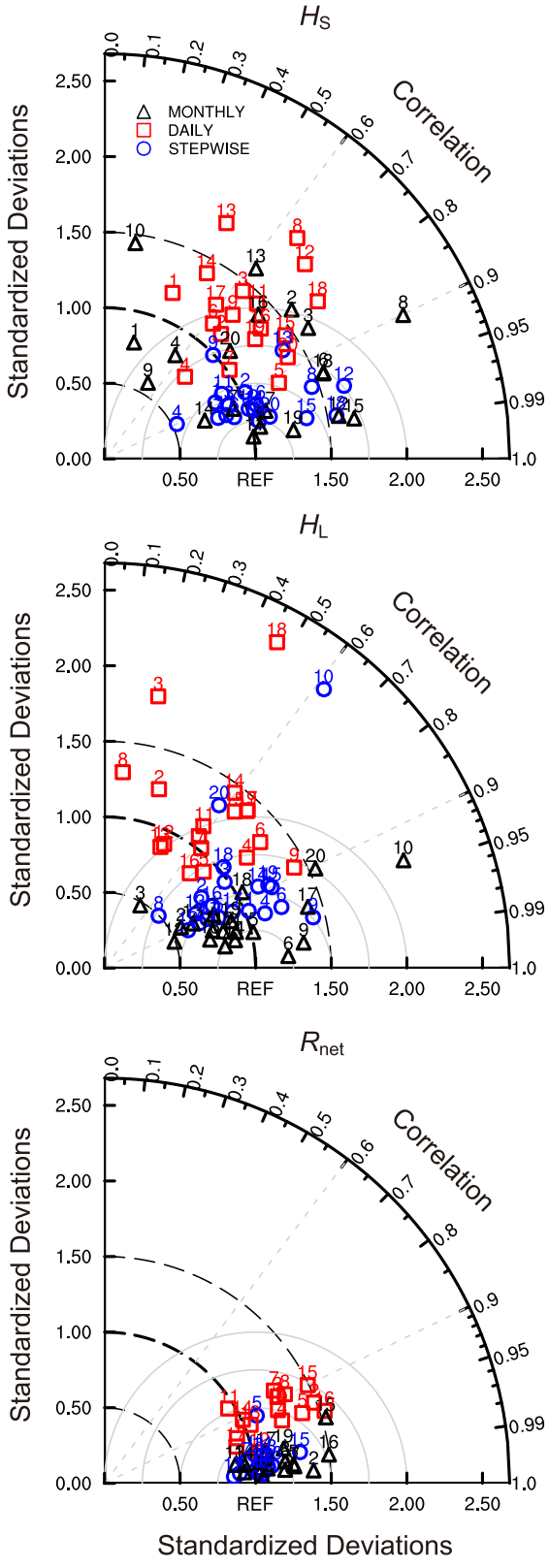

Fig. 1. Performance of CoLM simulations for eight land cover types (1, CRO; 2, DBF; 3, EBF; 4, ENF; 5, WET; 6, GRA; 7, MF; 8, SAV) and three variables: sensible heat flux (H_S); latent heat flux (H_L); and net radiation (R_{net}). Statistics are based on stepwise (X_s), daily (X_d), and monthly (X_m) simulated and observed H_S, H_L, and R_{net} results.

deviation) of H_S is higher than that of H_L, and the R range of H_L is smaller than that of H_S. Overall, CoLM simulates H_S, H_L, and R_{net} better at monthly and stepwise levels than it does at a daily scale, and produces a better simulation of H_L than H_S at all timescales.

The bold italic numbers in Table 2 show the best performances among the three timescales (the largest R or the smallest RMSE values of the four energy fluxes). Obviously, CoLM simulates the stepwise H_S better than its daily average and annual cycle in terms of the associated R values, and provides better simulations of H_L and H_G at the annual scale. An excellent performance in simulating R_{net} is observed at all three temporal scales, likely because the downward solar and longwave radiations are prescribed in the model.

Figure 2 compares the monthly averages of the energy fluxes between the model simulations and observations. Almost all modeled H_S values at the selected 20 sites follow the seasonal cycles of the observations, with bias varying by the different vegetation types. For example, the modeled H_S is lower than that of the observations for DBF and WET but higher for GRA, whereas the modeled H_L is higher than that of the observations for DBF and WET. The modeled H_L at all 20 sites, except for site US-Blo, follows the observed seasonal cycle and exhibits different biases for different vegetation types. The biases for both H_L and H_S are quite large in the wetlands (sites CA-Mer and FI-Kaa). H_S is overestimated during the dry periods at sites with typical dry and wet seasons, such as at US-Bkg, US-Var, and BW-Ma1.

Similar to the results of Stöckli et al. (2008), in our study, H_L is greater in magnitude than H_S at most sites. The simulated H_L is more consistent with the observed values than H_S in terms of both their magnitudes and temporal patterns. However, the fact that H_L is underestimated during dry periods whereas H_S is overestimated at sites with typical distinct dry and wet seasons, may be associated with the weakness of CoLM when simulating soil water in dry seasons. The deficiencies of the model in handling dry soil moistures may be caused by the lack of a full description of plant physiology—for example, the process of hydraulic redistribution (HR) (Burgess et al., 1998; Yan and Dickinson, 2014).

HR is defined as the passive water movement from wet soil to dry soil through plant roots, driven by water potential gradients. In the HR process, water can move passively through the roots, upwards or downwards, whenever a gradient in the soil water potential between soil layers exists and is stronger than the overall gradient between the soil and atmosphere (especially during the night, when transpiration is weak) (Oliveira et al., 2005). In dry seasons, HR allows water to move during the night or on cloudy days—specifically, from deep moist soil to dry shallow soil, where plant roots are more abundant. In wet seasons, water can also move down from the shallow layers to the deep layers via roots to reduce the loss through surface runoff or evaporation. HR has been recognized as a process that is widespread, occurs across several plant species and climates (Caldwell et al., 1998; Neumann and Cardon, 2012; Prieto et al., 2012; Quijano and Kumar, 2015), and may have an important influence on local and

Table 2. Performance of CoLM in simulating H_S, H_L, R_{net} and H_G on three timescales (stepwise, daily, and monthly). R and RMSE (W m^{-2}) were calculated for the eight land cover categories. Bold italic numbers indicate the best performance of the four energy fluxes, and the numbers inside brackets following the land-cover types represent the number of FLUXNET sites selected for the corresponding vegetation type. Some statistics are missing (–) owing to a lack of observations.

			CRO(1)	DBF(3)	EBF(1)	ENF(3)	WET(2)	GRA(4)	MF(1)	SAV(4)
R	Stepwise	H_S	0.89	0.91	***0.97***	0.95	0.58	0.92	0.94	0.96
		H_L	0.93	0.86	0.91	0.86	0.79	0.89	0.87	0.79
		H_G	0.76	0.12	0.46	0.60	–	0.73	–0.75	0.89
		R_{net}	***1.00***	***1.00***	0.91	***0.99***	–	***0.99***	***0.99***	***1.00***
	Daily	H_S	0.38	0.67	0.92	0.70	0.54	0.64	0.77	0.76
		H_L	0.58	0.43	0.72	0.50	0.63	0.53	0.67	0.56
		H_G	0.66	0.21	0.55	0.54	–	0.54	–0.64	0.72
		R_{net}	***0.95***	***0.92***	***0.94***	***0.89***	–	***0.91***	***0.95***	***0.94***
	Monthly	H_S	0.25	0.73	0.98	0.92	0.32	0.90	0.73	0.91
		H_L	0.90	0.78	0.97	0.64	0.97	0.94	0.97	0.92
		H_G	0.90	0.16	0.85	0.85	–	0.92	–0.96	0.81
		R_{net}	***1.00***	***1.00***	***0.99***	***0.99***	–	***0.99***	***0.99***	***0.98***
RMSE	Stepwise	H_S	29.28	45.48	29.29	38.24	49.08	32.31	33.31	37.92
		H_L	28.37	34.11	33.52	36.45	35.94	33.30	29.59	34.05
		H_G	24.49	28.10	***18.31***	18.29	–	36.17	32.84	***26.07***
		R_{net}	***13.22***	***19.34***	81.24	***15.90***	–	***29.71***	***22.97***	27.34
	Daily	H_S	10.43	13.98	9.46	12.21	19.51	12.73	13.32	10.41
		H_L	10.37	13.10	9.10	9.89	16.06	13.36	***10.02***	14.52
		H_G	5.82	***4.37***	***4.06***	***3.36***	–	7.41	10.30	***3.72***
		R_{net}	***4.41***	8.36	12.37	10.08	–	***7.15***	12.38	5.68
	Monthly	H_S	22.16	55.30	15.21	41.75	37.28	21.03	28.98	19.52
		H_L	16.83	25.38	15.70	22.76	26.29	19.72	14.43	13.01
		H_G	***3.82***	***4.27***	***2.44***	***2.59***	–	***3.32***	***17.89***	***3.57***
		R_{net}	5.47	27.21	16.12	29.49	–	21.34	26.48	15.32

global climate change (Lee et al., 2005; Wang et al., 2011).

Figure 3 shows the solar-normalized diurnal bias of H_S in different seasons. CoLM generates different magnitudes of biases in different seasons and exhibits different bias patterns for different vegetation types. It overestimates H_S for almost all eight vegetation types at noon during the summer (here, we took the summer season as June–July–August in the Northern Hemisphere, although three SAV sites and one EBF site in this study are located in the Southern Hemisphere, but these sites are located in either tropical or subtropical regions), except those in wetlands, and the U-shaped pattern of the normalized bias also exhibits relatively higher values when the downward solar radiation is higher. The biases of H_S show different patterns during different seasons, with magnitudes mostly within 10% of the solar radiation. Compared to the normalized diurnal bias of H_S, that of H_L exhibits a totally opposite pattern (Fig. 4), although the values fall within the range of 20% of the downward solar radiation.

A diurnal maximum bias occurs at noon, especially in the growing season, likely because CoLM could not explicitly capture the midday depression of the leaf gas exchange (Zeiger et al., 1987). A midday depression is one pattern of photosynthetic diurnal variation, with two marked peaks that occur in the late morning and late afternoon, separately (Pessarakli, 2005); this pattern occurs in many plants and will have a significant impact on crop yields. The physiological factors responsible for the midday depression consist of stomatal closure, the enhancement of respiration and photorespiration, an increase in the mesophyll resistance of CO_2, and a decrease in the leaf water potential. However, the stomatal resistance in CoLM is coupled with leaf photosynthesis in a manner similar to that described by Collatz et al. (1991) and does not consider the mesophyll diffusion of CO_2. All of these deficiencies in simulating the leaf gas exchange may cause a bias in simulating H_L because one important part of H_L is transpiration [see Eq. (6)], and the calculation of transpiration relies on stomatal resistance and leaf boundary layer resistance.

In CoLM, the H_G at the land surface is computed as the residual of the net radiation, based on the energy balance equation: $H_G = R_{net} - H_S - H_L$ (Dai et al., 2003). The discrepancy between the simulated and observed H_G (Fig. 2c) indicates the embedded errors of estimating H_S and H_L using the simulated H_G. CoLM produces a positive H_G bias during daytime and a negative H_G bias at night. The bias does not exhibit any seasonal dependence (not shown).

A satisfactory agreement is found between the observed and simulated net radiation (Fig. 2d and Table 2), with R shown in the Taylor diagram. The high-quality simulation of the net radiation may be the result of the prescribed down-

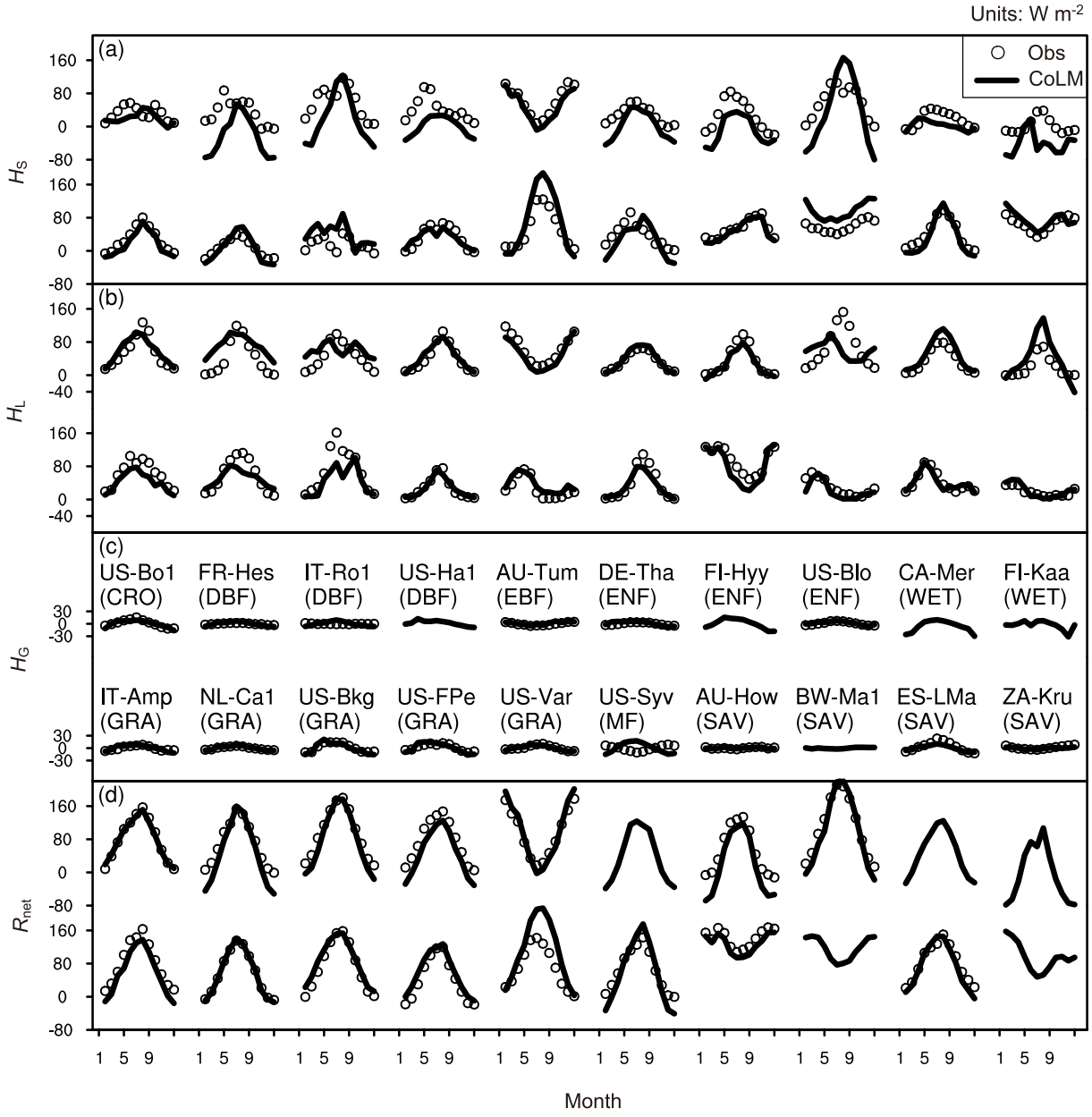

Fig. 2. Annual cycles of observed (Obs, black circles) and simulated (CoLM, black line) (a) H_S, (b) H_L, (c) H_G and (d) R_{net} at the 20 FLUXNET sites, with their names and plant functional types denoted in panel (c).

ward solar and longwave radiation and the accurate estimates of the surface albedo in the model.

3.2. *Different vegetation types*

The 20 selected sites in this study cover eight vegetation types to provide useful comparisons. Table 3 lists the means of the simulated biases of the four energy fluxes over different vegetation types. CoLM underestimates H_S for more than half of these eight vegetation types and exhibits a negative H_L bias for CRO, GRA, and SAV, and a positive bias for the other five types. Similarly, CoLM exhibits a negative R_{net} bias for EBF, DBF, and SAV, and a positive bias for the other

Table 3. Mean normalized simulation bias by vegetation type. Some statistics are missing (–) owing to a lack of observations.

	CRO(1)	DBF(3)	EBF(1)	ENF(3)	WET(2)	GRA(4)	MF(1)	SAV(4)
H_S	−0.01	−0.24	−0.02	0.03	0.50	0.06	−0.08	−0.04
H_L	−0.02	0.10	0.01	0.03	0.09	−0.09	0.04	−0.03
H_G	0.13	0.20	0.02	0.09	–	0.28	0.06	0.09
R_{net}	0.09	−0.01	−0.07	0.24	–	0.18	0.12	−0.03

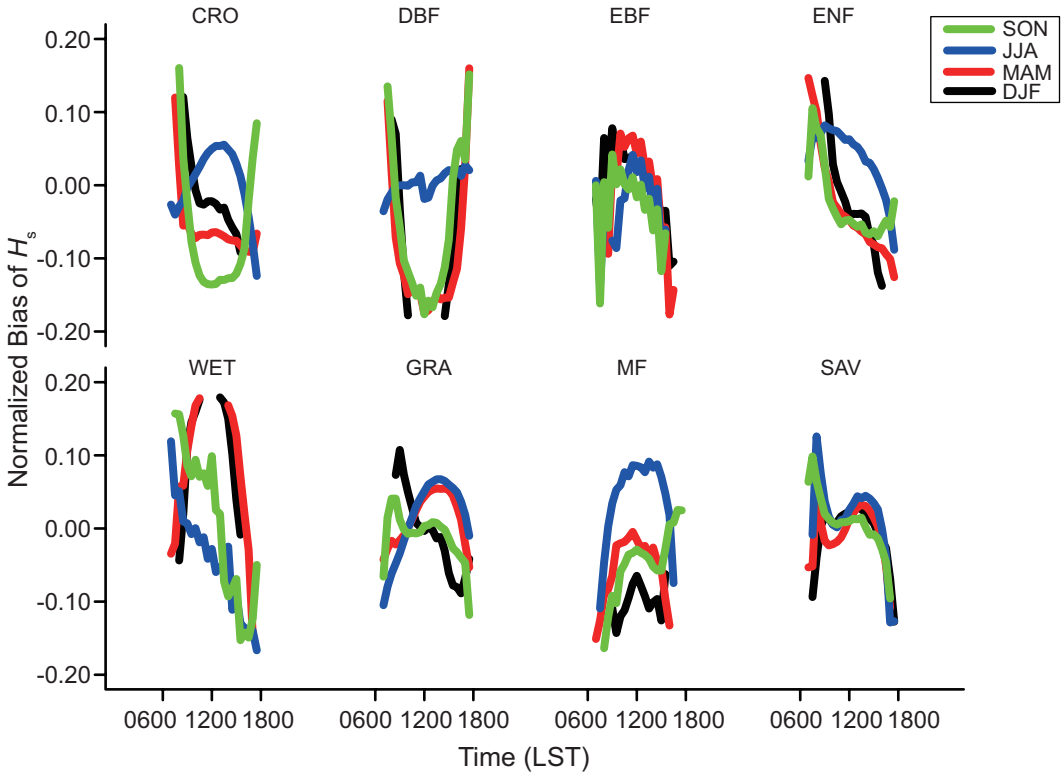

Fig. 3. Normalized diurnal bias of H_S over eight different vegetation types in different seasons: red for spring (March–April–May, MAM); blue for summer (June–July–August, JJA); green for autumn (September–October–November, SON); black for winter (December–January–February, DJF).

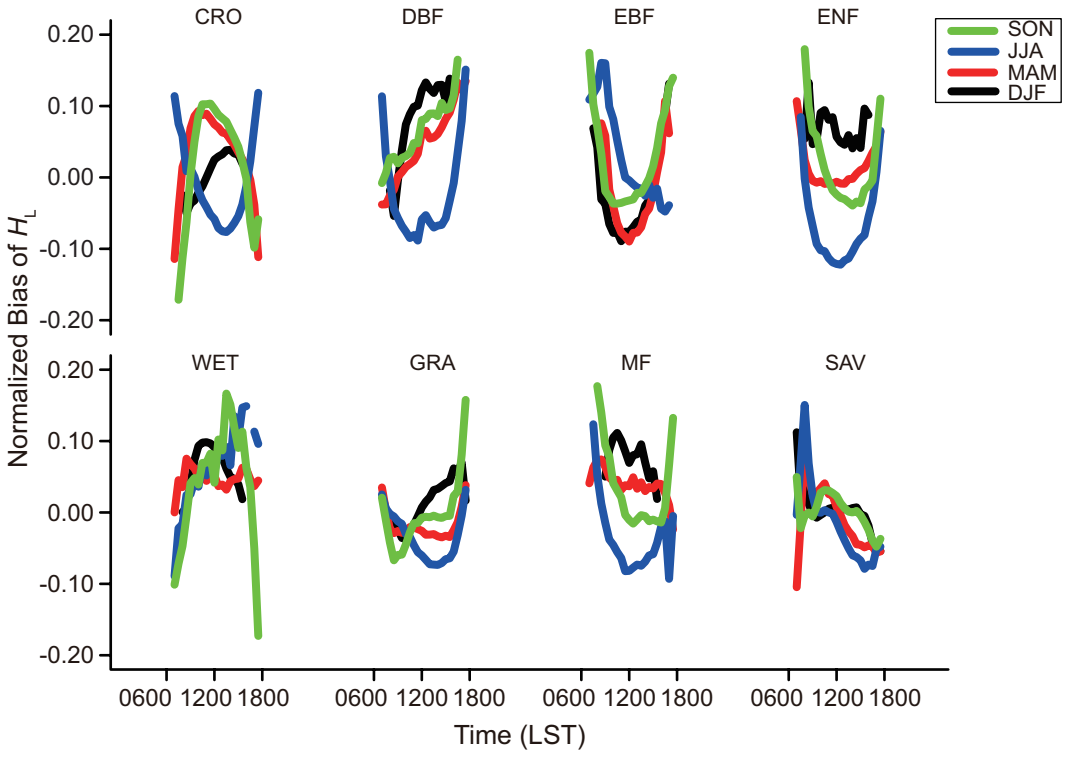

Fig. 4. As in Fig. 3 but for H_L.

land-cover types. Although H_G is small in the energy balance equilibrium, its simulation error may not be negligible compared to the other three fluxes.

3.2.1. *Deciduous Broadleaf Forest*

DBF covers most of the eastern United States, central and northern Europe, eastern China, and Japan. It has a long warm growing season. In this study, the three DBF sites are in temperate (FR-Hes), subtropical-Mediterranean (IT-Ro1), and temperate-continental with warm summers (US-Ha1) climate zones. Interestingly, despite the climate discrepancies (site IT-Ro1 is hotter and drier in the summer than FR-Hes and US-Ha1, and US-Ha1 has a colder winter) and because of the abundant moisture in DBF, CoLM underestimates H_S and overestimates H_L at all three sites, based on the monthly N_{bias}.

According to Stöckli et al. (2008), CLM3.0 overestimates H_L in the winter but underestimates it in the summer. CoLM yields analogous seasonal performances. From the seasonality evident in Fig. 2, one can identify that the simulated H_L exhibits a high consistency with the observations for the temperate-continental with warm summers (US-Ha1) climate zone. CoLM generates negative H_L errors for the temperate (FR-Hes) zone and an H_L phase error for the subtropical-Mediterranean (IT-Ro1) zone.

At the stepwise scale, the R values of H_S at the three DBF sites (0.90, 0.92, and 0.90 for FR-Hes, IT-Ro1, and US-Ha1, respectively) indicate a better performance of CoLM in simulating H_L (0.81, 0.81, and 0.95, respectively). However, the simulated H_S is not always better than the simulated H_L at the monthly scale (R of H_S is 0.78, 0.84, and 0.56, while that of H_L is 0.88, 0.50, and 0.96). Therefore, CoLM can achieve a good performance in terms of modeling H_S and H_L at different timescales, even for the same vegetation type. Given the seasonal precipitation patterns of the three sites, it is obvious that the CoLM conducts better simulations at sites with even monthly rainfall, such as that of the temperate-continental climate zone.

3.2.2. *Evergreen Needleleaf Forest*

Woody plants cover more than 60% of ENF zones, and their canopies are normally higher than 2 m. Almost all trees remain green year-round in ENFs. The selected ENF sites in this study are located in temperate (DE-Tha), boreal (FI-Hyy), and subtropical-Mediterranean (US-Blo) climate zones. Obviously, the site US-Blo is the warmest and has the most abundant precipitation, while DE-Tha is warmer than FI-Hyy. However, site US-Blo has distinct dry and wet seasons.

CoLM performs better when simulating H_S than when simulating H_L at the three ENF sites, based on a stepwise R analysis, and all of the R values of H_S at the three sites (0.96, 0.94, and 0.94 for DE-Tha, FI-Hyy, US-Blo) are higher than those of H_L (0.95, 0.90, and 0.72). Although CoLM overestimates H_L, with a mean normalized stepwise bias of 0.05, 0.02, and 0.03, it underestimates H_S at DE-Tha (-0.06) and FI-Hyy (-0.03), and overestimates H_S at US-Blo (0.05).

CoLM produces the best H_L seasonal cycles at DE-Tha and FI-Hyy (see Fig. 2b), and produces a phase error at site US-Blo. While the model captures the general pattern of the H_S seasonal cycle, it underestimates the annual range of H_S at sites DE-Tha and FI-Hyy, and generates a greater range of simulated H_S values than those observed.

Yang et al. (2009) noted that the soil surface resistance controls the surface evaporation of alpine deserts, but is not reasonably implemented in CoLM. After adjusting the soil porosity, hydraulic conductivity of saturated soil, and vertical soil layering scheme, Li et al. (2012) found that CoLM could simulate the soil moisture distribution at three stations on the Tibetan Plateau. The lack of these adjustments may be the reason why CoLM could not yield satisfactory performances at US-Blo. Based on the literature and our experiments, we infer that high spatiotemporal resolution land surface data (Yuan et al., 2011; Shangguan et al., 2014) will improve the performance of CoLM.

3.2.3. *Grassland*

GRA is the land cover type that is dominated by herbaceous plants. The temperature varies more strongly from summer to winter, and the annual precipitation is lower in the temperate grasslands than in the savannas. Sites from subtropical-Mediterranean (IT-Amp and US-Var), temperate (NL-Ca1), temperate-continental with hot summers (US-Bkg), and dry (US-FPe) zones are used for the representations of GRA.

From the results of the R and RMSE calculations, CoLM performs consistent well at IT-Amp and NL-Ca1 at the monthly scale, with larger R and smaller RMSE values for H_S than those for H_L, and at US-FPe, it exhibits the opposite pattern. At the daily timescale, CoLM exhibits consistently better performance in predicting H_S at NL-Ca1 and US-Bkg. Interestingly, the hourly R and RMSE values indicate consistently better simulations of H_S at NL-Ca1 alone. Based on the N_{bias} results, CoLM consistently underestimates H_L at all three timescales for IT-Amp, and consistently overestimates H_L for US-Var. The different performances at the different timescales between these five sites and the different performances for the different sites from the different climate zones at the same timescales suggest that, for the same land-cover types, different climate conditions can affect the performance of the model.

3.2.4. *Savanna*

SAV describes grasslands with scattered individual trees and porous soil, favoring the rapid drainage of water. SAV has both dry and rainy seasons. Sites representing the SAV land-cover type were from tropical (AU-How), dry (BW-Ma1), and subtropical-Mediterranean (ES-LMa and ZA-Kru) zones.

Similar to those of GRA, the R and N_{bias} exhibit consistent patterns for SAV in the different climate zones for the three timescales. For example, the monthly R at site ZA-Kru exhibits the same improved performance for the simulation of H_S as its performance for the simulation of H_L, which is also

exhibited in the hourly simulations at sites AU-How and ES-LMa and the daily simulations at sites BW-Ma1, ES-LMa, and ZA-Kru. The hourly and monthly $N_{\rm bias}$ values are consistent for the simulated $H_{\rm S}$, which is opposite to the behavior seen in the daily simulations.

Given the different characteristics of these land-cover types, i.e., GRA and SAV differ in their surface roughness, zero-plane displacement, and soil parameters (e.g., root depth and coefficient of root profile), CoLM achieves different performances even for these two more-similar vegetation types. Groenendijk et al. (2011) noted that the quality of the fluxes decrease when more general parameters are used because the choice of a parameter classification has a considerable impact on the quality of the simulated photosynthesis and transpiration fluxes.

4. Discussion and conclusions

This study evaluated the performance of CoLM in simulating energy fluxes across a global range of ecosystems, over eight vegetation types within ten subclasses of climate zones. The utilization of the decomposition method provided detailed information that could be used to assess the performance of the model on different timescales, and the correction method effectively served as the energy closure of the eddy covariance measurement. The simulated energy fluxes were first evaluated over different timescales for eight land-cover types, and then for certain land-cover types in different climate zones. Overall, the results demonstrate that CoLM generally exhibits a satisfactory modeling performance.

Of the four energy fluxes, CoLM generally exhibits better performance for $H_{\rm L}$ than for $H_{\rm S}$, based on the Taylor diagram, and performs well in simulating the seasonality at the 20 sites selected in this study. A strong agreement between the simulations and observational data is found in the seasonal cycle of $R_{\rm net}$. $H_{\rm L}$ is underestimated during dry periods at sites with distinct dry and wet seasons, and $H_{\rm S}$ is overestimated, which might be related to the weakness of the model when simulating soil water during dry seasons.

At the diurnal scale, CoLM produces a maximum bias close to noon in the summer, and the bias varies between different vegetation types and climate zones. This provides modelers with a clue for how to improve the ability of the model to simulate the midday depression of leaf gas exchange. Given the physical factors that lead to this midday depression, the model performance may be improved by explicitly implementing the stomatal closure mechanism or incorporating mesophyll diffusion in the sub-model of photosynthesis.

Regarding the different vegetation types, CoLM performs best for EBF among the eight vegetation types and worst for CRO and WET. Although different climate conditions will lead to different model behavior, even for the same land-cover type, CoLM produces better simulations for sites with even monthly rainfall.

All three indexes utilized in this study—R, RMSE, and $N_{\rm bias}$—do not show a consistent model performance between different energy fluxes, different timescales of certain sites, or different climate zones of one land-cover type. Therefore, it is difficult to assess the model's merits and limitations using a particular single index. We should combine the different skills of these indexes when evaluating the model's performance.

Based on earlier studies and our evaluation, the implementation of site-specific parameters, including soil porosity, hydraulic conductivity of saturated soil, and a vertical soil layering scheme, will significantly improve the performance of CoLM, whereas a more general classification of the implemented parameters will reduce the predicted fluxes. For global-scale simulations, high-resolution datasets of land-surface characteristics are needed to achieve high-accuracy results.

Overall, CoLM simulates energy fluxes better at monthly and stepwise scales than at daily scales, and it underestimates $H_{\rm S}$ and overestimates $H_{\rm L}$ for most of the 20 sites selected in this study. CoLM performs best for the EBF vegetation type, and worst for CRO and WET. The reason why CoLM underestimates $H_{\rm L}$ at some sites may be associated with its weakness in simulating soil water in dry seasons. In addition, the model's deficiencies in simulating the midday depression of leaf gas exchange may account for the maximum bias observed at noon in summer, which is a potential subject for future research.

Acknowledgements. This work was supported by the R&D Special Fund for Nonprofit Industry (Meteorology) (Grant Nos. GYHY200706025, GYHY201206013 and GYHY201306066). We thank the two reviewers for their time and effort to thoroughly review the manuscript. Their suggestions greatly improved the paper.

REFERENCES

Aitken, A. P., 1973: Assessing systematic errors in rainfall-runoff models. *J. Hydrol.*, **20**, 121–136, doi: 10.1016/0022-1694(73)90035-8.

Baldocchi, D., and Coauthors, 2001: FLUXNET: A new tool to study the temporal and spatial variability of ecosystem-scale carbon dioxide, water vapor, and energy flux densities. *Bull. Amer. Meteor. Soc.*, **82**, 2415–2434, doi: 10.1175/1520-0477(2001)082<2415:FANTTS>2.3.CO;2.

Baldocchi, D., and Coauthors, 2016: Role of flux networks in benchmarking land atmosphere models. *2016 International Land Model Benchmarking (ILAMB) Workshop*, Washington, DC, ILAMB.

Best, M., and Coauthors, 2015: The plumbing of land surface models: Benchmarking model performance. *Journal of Hydrometeorology*, **16**, 1425–1442, doi: 10.1175/JHM-D-14-0158.1.

Blyth, E., J. Gash, A. Lloyd, M. Pryor, G. P. Weedon, and J. Shuttleworth, 2010: Evaluating the JULES land surface model energy fluxes using FLUXNET data. *Journal of Hydrometeorology*, **11**, 509–519, doi: 10.1175/2009JHM1183.1.

Bonan, G. B., 1996: A Land Surface Model (LSM Version 1.0) for Ecological, Hydrological, and Atmospheric Studies: Technical Description and User's Guide. NCAR Tech. Note NCAR/

TN-417+STR, 150 pp.

Bonan, G. B., 2015: *Ecological Climatology: Concepts and Applications*. 3rd ed., Cambridge University Press.

Bonan, G. B., K. W. Oleson, M. Vertenstein, S. Levis, X. B. Zeng, Y. J. Dai, R. E. Dickinson, and Z. L. Yang, 2002: The land surface climatology of the community land model coupled to the NCAR community climate model. *J. Climate*, **15**, 3123–3149, doi: 10.1175/1520-0442(2002)015<3123:TLSCOT>2.0.CO;2.

Burgess, S. S. O., M. A. Adams, N. C. Turner, and C. K. Ong, 1998: The redistribution of soil water by tree root systems. *Oecologia*, **115**, 306–311, doi: 10.1007/s004420050521.

Caldwell, M. M., T. E. Dawson, and J. H. Richards, 1998: Hydraulic lift: Consequences of water efflux from the roots of plants. *Oecologia*, **113**, 151–161, doi: 10.1007/s004420050363.

Collatz, G. J., J. T. Ball, C. Grivet, and J. A. Berry, 1991: Physiological and environmental regulation of stomatal conductance, photosynthesis and transpiration: A model that includes a laminar boundary layer. *Agricultural and Forest Meteorology*, **54**, 107–136, doi: 10.1016/0168-1923(91)90002-8.

Dai, Y. J., and Q. C. Zeng, 1997: A land surface model (IAP94) for climate studies part I: Formulation and validation in offline experiments. *Adv. Atmos. Sci.*, **14**, 433–460, doi: 10.1007/s00376-997-0063-4.

Dai, Y. J., and Coauthors, 2003: The common land model. *Bull. Amer. Meteor. Soc.*, **84**, 1013–1023, doi: 10.1175/BAMS-84-8-1013.

Dai, Y. J., R. E. Dickinson, and Y.-P. Wang, 2004: A two-big-leaf model for canopy temperature, photosynthesis, and stomatal conductance. *J. Climate*, **17**, 2281–2299, doi: 10.1175/1520-0442(2004)017<2281:ATMFCT>2.0.CO;2.

Dickinson, R. E., A. Henderson-Sellers, P. J. Kennedy, and M. F. Wilson, 1986: Biosphere-Atmosphere Transfer Scheme (BATS) for the NCAR Community Climate Model. NCAR Tech. Note NCAR/TN-275-+STR, doi: 10.5065/D6668B58.

Groenendijk, M., and Coauthors, 2011: Assessing parameter variability in a photosynthesis model within and between plant functional types using global FLUXNET eddy covariance data. *Agricultural and Forest Meteorology*, **151**, 22–38, doi: 10.1016/j.agrformet.2010.08.013.

Henderson-Sellers, A., Z. L. Yang, and R. E. Dickinson, 1993: The project for intercomparison of land-surface parameterization schemes. *Bull. Amer. Meteor. Soc.*, **74**, 1335–1349, doi: 10.1175/1520-0477(1993)074<1335:TPFIOL>2.0.CO;2

Huang, C. L., X. Li, and J. Gu, 2008: Estimation of regional soil moisture by assimilating multi-sensor passive microwave remote sensing observations based on ensemble Kalman filter. *Proc. IEEE International Geoscience and Remote Sensing Symposium*, Boston, MA, IEEE, III-1052–III-1055, doi: 10.1109/IGARSS.2008.4779534.

James, L. D., and S. J. Burges, 1982: Selection, calibration, and testing of hydrologic models. *Hydrologic Modelling of Small Watersheds*, C. T. Haan, Ed., ASAE Michigan, 435–472.

Ji, D., and Coauthors, 2014: Description and basic evaluation of BNU-ESM version 1. *Geosci. Model Dev. Discuss.*, **7**, 1601–1647, doi: 10.5194/gmdd-7-1601-2014.

Jung, M., and Coauthors, 2010: Recent decline in the global land evapotranspiration trend due to limited moisture supply. *Nature*, **467**, 951–954, doi: 10.1038/nature09396.

Kottek, M., J. Grieser, C. Beck, B. Rudolf, and F. Rubel, 2006: World map of the Köppen-Geiger climate classification updated. *Meteor. Z.*, **15**, 259–263, doi: 10.1127/0941-2948/2006/0130.

Lee, J.-E., R. S. Oliveira, T. E. Dawson, and I. Fung, 2005: Root functioning modifies seasonal climate. *Proceedings of the National Academy of Sciences of the United States of America*, **102**, 17 576–17 581, doi: 10.1073/pnas.0508785102.

Li, Y., X. Liu, and W. P. Li, 2012: Numerical simulation of land surface process at different underlying surfaces in Tibetan Plateau. *Plateau Meteorology*, **31**, 581–591. (in Chinese)

Luo, Y. Q., and Coauthors, 2012: A framework for benchmarking land models. *Biogeosciences*, **9**, 3857–3874, doi: 10.5194/bg-9-3857-2012.

Ma, L. L., L. L. Tang, and Z. L. Li, 2006: Simulation of land ETs of China with CoLM. *Proc. SPIE 6200, Remote Sensing of the Environment: 15th National Symposium on Remote Sensing of China*, Guiyan City, China, SPIE, 62000N, doi: 10.1117/12.681768.

Meng, C. L., Z. L. Li, X. Zhan, J. C. Shi, and C. Y. Liu, 2009: Land surface temperature data assimilation and its impact on evapotranspiration estimates from the Common Land Model. *Water Resour. Res.*, **45**, W02421, doi: 10.1029/2008WR006971.

Neumann, R. B., and Z. G. Cardon, 2012: The magnitude of hydraulic redistribution by plant roots: A review and synthesis of empirical and modeling studies. *New Phytologist*, **194**, 337–352, doi: 10.1111/j.1469-8137.2012.04088.x.

Oleson, K. W., and Coauthors, 2008: Improvements to the Community Land Model and their impact on the hydrological cycle. *J. Geophys. Res.*, **113**(G1), G01021, doi: 10.1029/2007JG000563.

Oleson, K. W., and Coauthors, 2013: Technical Description of Version 4.5 of the Community Land Model (CLM). NCAR Tech. Note NCAR/TN-503+STR, 420 pp, doi: 10.5065/D6RR1W7M.

Oliveira, R. S., T. E. Dawson, S. S. O. Burgess, and D. C. Nepstad, 2005: Hydraulic redistribution in three Amazonian trees. *Oecologia*, **145**, 354–363, doi: 10.1007/s00442-005-0108-2.

Pessarakli, M., 2005: *Handbook of Photosynthesis*. 2nd ed., CRC Press.

Prieto, I., C. Armas, and F. I. Pugnaire, 2012: Water release through plant roots: New insights into its consequences at the plant and ecosystem level. *New Phytologist*, **193**, 830–841, doi: 10.1111/j.1469-8137.2011.04039.x.

Quijano, J. C., and P. Kumar, 2015: Numerical simulations of hydraulic redistribution across climates: The role of the root hydraulic conductivities. *Water Resour. Res.*, **51**, 8529–8550, doi: 10.1002/2014WR016509.

Roerink, G. J., Z. Su, and M. Menenti, 2000: S-SEBI: A simple remote sensing algorithm to estimate the surface energy balance. *Physics and Chemistry of the Earth, Part B: Hydrology, Oceans and Atmosphere*, **25**, 147–157, doi: 10.1016/S1464-1909(99)00128-8.

Sellers, P. J., and Coauthors, 1997: Modeling the exchanges of energy, water, and carbon between continents and the atmosphere. *Science*, **275**, 502–509, doi: 10.1126/science.275.5299.502.

Shangguan, W., Y. J. Dai, Q. Y. Duan, B. Y. Liu, and H. Yuan, 2014: A global soil data set for earth system modeling. *Journal of Advances in Modeling Earth Systems*, **6**, 249–263, doi: 10.1002/2013MS000293.

Stöckli, R., and Coauthors, 2008: Use of FLUXNET in the community land model development. *J. Geophys. Res.*, **113**,

G01025, doi: 10.1029/2007JG000562.

Taylor, K. E., 2001: Summarizing multiple aspects of model performance in a single diagram. *J. Geophys. Res*., **106**, 7183–7192, doi: 10.1029/2000JD900719.

Twine, T. E., and Coauthors, 2000: Correcting eddy-covariance flux underestimates over a grassland. *Agricultural and Forest Meteorology*, **103**, 279–300, doi: 10.1016/S0168-1923(00)00123-4.

Wang, G. L., C. Alo, R. Mei, and S. S. Sun, 2011: Droughts, hydraulic redistribution, and their impact on vegetation composition in the Amazon forest. *Plant Ecology*, **212**, 663–673, doi: 10.1007/s11258-010-9860-4.

Wilson, K., and Coauthors, 2002: Energy balance closure at FLUXNET sites. *Agricultural and Forest Meteorology*, **113**, 223–243, doi: 10.1016/S0168-1923(02)00109-0.

Xin, Y. F., L. G. Bian, and X. H. Zhang, 2006: The application of CoLM to arid region of Northwest China and Qinghai-Xizang Plateau. *Plateau Meteorology*, **25**, 567–574, doi: 10.3321/j.issn:1000-0534.2006.04.002. (in Chinese)

Xu, T. R., S. L. Liang, and S. M. Liu, 2011: Estimating turbulent fluxes through assimilation of geostationary operational environmental satellites data using ensemble Kalman filter. *J. Geophys. Res*., **116**, D09109, doi: 10.1029/2010JD015150.

Yan, B. Y., and R. E. Dickinson, 2014: Modeling hydraulic redistribution and ecosystem response to droughts over the Amazon basin using Community Land Model 4.0 (CLM4). *J. Geophys. Res*., **119**, 2130–2143, doi: 10.1002/2014JG002694.

Yang, K., Y. Y. Chen, and J. Qin, 2009: Some practical notes on the land surface modeling in the Tibetan Plateau. *Hydrology and Earth System Sciences*, **13**, 687–701, doi: 10.5194/hess-13-687-2009.

Yuan, H., Y. J. Dai, Z. Q. Xiao, D. Y. Ji, and W. Shangguan, 2011: Reprocessing the MODIS Leaf Area Index products for land surface and climate modelling. *Remote Sensing of Environment*, **115**, 1171–1187, doi: 10.1016/j.rse.2011.01.001.

Zeiger, E., G. D. Farquhar, and I. R. Cowan, 1987: *Stomatal Function*. Stanford University Press.

Zeng, X. B., M. Shaikh, Y. J. Dai, R. E. Dickinson, and R. Myneni, 2002: Coupling of the common land model to the NCAR community climate model. *J. Climate*, **15**, 1832–1854, doi: 10.1175/1520-0442(2002)015<1832:COTCLM>2.0.CO;2.

Zhang, S. W., D. Q. Li, and C. J. Qiu, 2011: A multimodel ensemble-based Kalman filter for the retrieval of soil moisture profiles. *Adv. Atmos. Sci*., **28**, 195–206, doi: 10.1007/s00376-010-9200-6.

Zheng, J., Z. H. Xie, Y. J. Dai, X. Yuan, and X. Q. Bi, 2009: Coupling of the common land model (CoLM) with the regional climate model (RegCM3) and its preliminary validation. *Chinese Journal of Atmospheric Sciences*, **33**, 737–750, doi: 10.3878/j.issn.1006-9895.2009.04.08. (in Chinese)